Conf-9108180--1

PPPL-CFP--2467

DE92 001839

Analysis Techniques for Momentum Transport presented at III Workshop on Magnetic Confinement Fusion: Improved Confinement in Tokamaks and Stellerators 26-30 August 1991 Santander, Spain

S.D. Scott

Plasma Physics Laboratory
Princeton University
Princeton, NJ, USA 08543

1. The momentum balance equation

The basic momentum-balance equation that is used to infer local values of the momentum diffusivity (χ_ϕ) from measurements of the rotation speed is [1]

$$
\begin{aligned}
\frac{\partial}{\partial t}(\sum_j n_j m_j R^2 \omega_\phi) \quad = \quad & T_{col} \quad \text{(collisonal torque from beams)} \qquad (1) \\
& + T_{bth} \quad \text{(beam thermalization torque)} \\
& + T_{iz} \quad \text{(torque from ionization of rotating neutrals)} \\
& + \nabla \cdot \sum_j n_j m_j R^2 \chi_{\phi_j} \nabla \omega_\phi \quad \text{(viscous torque)} \\
& - \nabla \cdot \sum_j m_j \Gamma_j R \omega_\phi \quad \text{(torque convection)} \\
& - \sum_j n_j m_j R \omega_\phi (\frac{1}{\tau_{\phi cx}} + \frac{1}{\tau_{\phi\delta}}). \quad \text{(charge-exchange, ripple)}
\end{aligned}
$$

Generally the densities and rotation frequencies are measured, the torque densities are calculated from a beam code, and the equation is solved for $\chi_\phi(r,t)$. The magnitude of the convection term is somewhat arbitrary – the choice made in Eq. 1 is that each ion convected across a flux surface carries with it the local rotation speed. The turbulence which actually drives cross-field transport might well impose a different multiplier. The Γ_j terms are the radial fluxes of each ion species, which are determined separately from the particle continuity equation. The assumption has been made that all the ions rotate at the same rotation speed, which may not be valid in all regimes [2].

The principle objective of performing momentum transport analysis is to identify the behavior of the momentum diffusivity χ_ϕ, in particular its variation with various plasma parameters. A wide variety of experiments has found that χ_ϕ behaves similarly to the heat transport coefficients χ_i and χ_e, and it seems reasonable to assume that a common mechanism controls transport of both heat and momentum.

Studies of momentum transport offer the following advantages with respect to studies of heat transport:

- Ion-electron coupling is negligible in the momentum equation, due to the small electron mass. This allows χ_ϕ to be determined accurately in low-temperature plasmas where it is difficult to separate χ_i from χ_e.

- The convection term remains reasonably small even in the center of very hot plasmas, so that uncertainties in its magnitude don't introduce large errors into the inferred χ_ϕ. By contrast, heat convection becomes the dominant term in the power balance.

- If both co- and counter-beams are available, the torque can be varied with other conditions (in particular, beam power) held constant.
- In plasmas with modest Z_{eff} (≥ 2) and strong beam heating, the thermal ion density ($n_i \equiv n_e - n_z Z - n_{\text{beam}}$) can become a small fraction of n_e, and its magnitude quite uncertain. The plasma *mass density*, which enters the momentum balance equation, remains more constant under these conditions.
- Rotation is generally easier to measure than temperature, because the rotation measurement is derived from the position of the *centroid* of a shifted impurity radiation line, while the temperature is derived from a measurement of the line *width*.

One limitation of momentum transport analysis, from the point of view of understanding anomalous transport, is that additional torques can be imposed on a plasma through radial currents ($\vec{J}_r \times \vec{B}_\theta$) that are not measured. For example, toroidal rotation has been observed to *stop* in JET with up to 10 MW of co-injection power during 'locked modes'. Although degradation of energy confinement is also observed with locked modes ($\leq 30\%$), it is not as severe as the total loss of rotation. It has been conjectured that the rotation damping results from an electromagnetic interaction between the internal modes and eddy currents in the vessel wall, or with fixed stray fields [3]. Similar observations have been reported by the ASDEX group [4].

Similarly, toroidal rotation appears to slow down if ICRF power is added to a beam-heated discharge. This effect has apparently not been studied systematically, but could be due to a radial current of energetic ions driven by the RF [5]. Unless these radial currents (if present) are understood, the momentum transport analysis will erroneously infer a change in χ_ϕ where it in fact remained constant.

1.1. Typical analysis

Figures 2 and 3 show a typical momentum transport analysis for a strongly co- -rotating TFTR plasma (12 MW co-injection, low-recycling, $T_i \approx 20$ keV, $T_e(0) \approx 7$ keV). The $\vec{J} \times \vec{B}$ torque is reasonably small because injection was in the co-direction. Due to the high central ion temperatures, the beam thermalization torque dominates at the plasma center. The ion thermal density is reasonably small due to carbon contamination ($Z_{\text{eff}}= 3.6$) and the large beam-ion population; the carbon impurity contributes about half the plasma mass. Note that viscous damping is the dominant term in the momentum balance over the entire plasma; convection remains small even at the plasma center. By contrast, in the power balance analysis heat convection (assuming $q = \frac{3}{2}\Gamma T$) becomes larger than heat conduction for both ions and electrons inside of $r \leq 34$ cm. The inferred momentum diffusivity χ_ϕ increases strongly with radius. The decrease in χ_i and χ_e near the plasma center

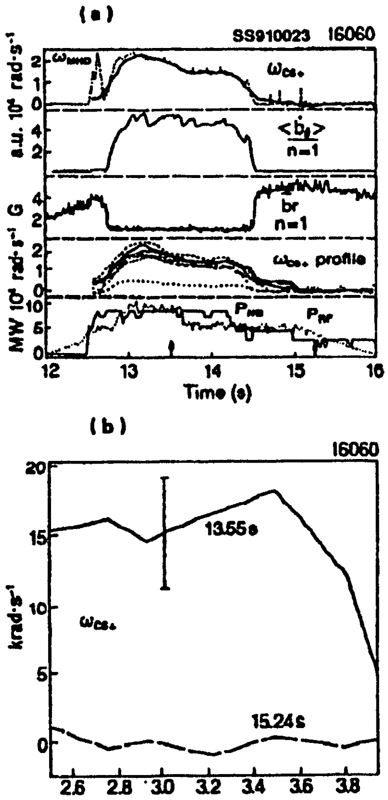

Figure 1: Effect of mode locking on toroidal rotation observed in JET [3]. An $m = 2$, $n = 1$ was locked before NBI started, then it unlocked for ~2.5 s. It locked once again at ~14.5 s, shortly after the beam power was reduced below 5 MW. Note the excellent agreement between the angular rotation frequency measured by CXR and the MHD frequency. The rotation profile was quite flat inside the $R = 3.8$ m location (the calculated radius of the $q = 2$ surface was ~3.9 m) during the $m = 2$ MHD, then it fell to near zero across the entire profile when the mode locked. Near-zero rotation speeds have been observed during locked modes even at neutral beam powers of 10 MW.

is even more pronounced, but there the analysis is uncertain due to the convection term.

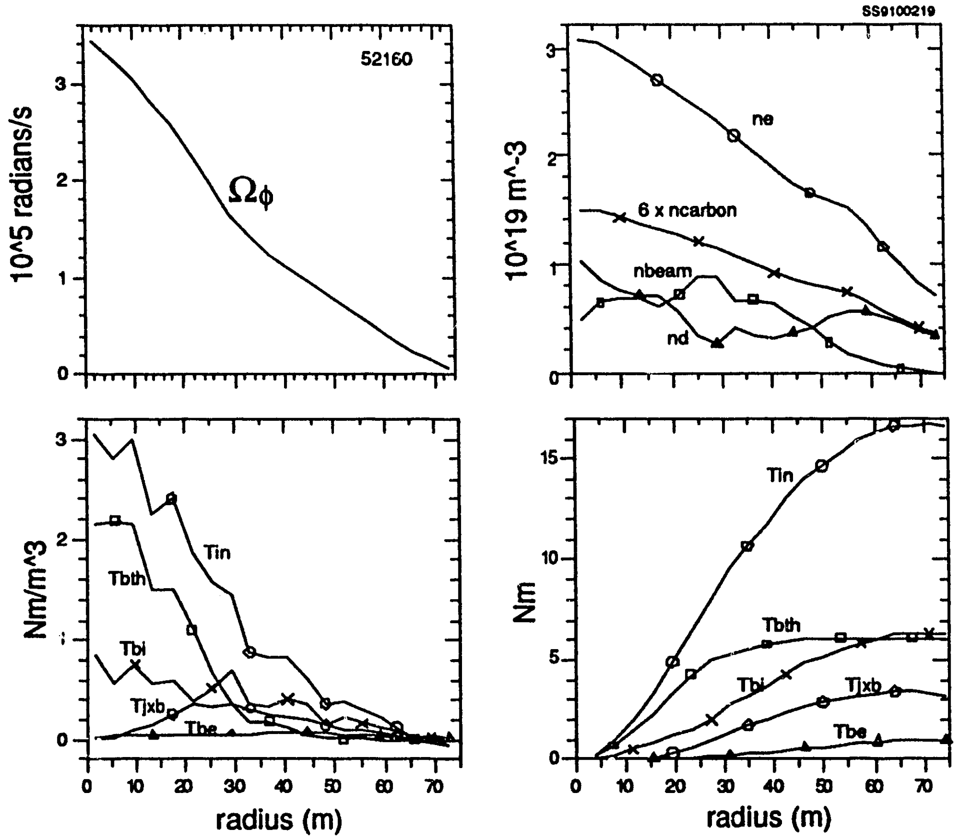

Figure 2: Measured and calculated inputs to the momentum transport analysis for a strongly rotating TFTR plasma. The carbon density has been multiplied by 6 to show its relative contribution to the plasma mass density. The torque densities were calculated by a Monte Carlo routine in the TRANSP code.

1.2. analysis difficulties for χ_i and χ_e at low temperature

At the low T_e obtained in L-mode plasmas, the electron-ion power coupling ($q_{ei} \propto n_e^2 Z_{eff}(T_e - T_i)/T_e^{3/2}$) is large even for modest temperature differences ($T_e - T_i$). Consequently, T_i cannot differ significantly from the T_e – otherwise there would be more power flowing from electrons to ions (or vice versa) than is available from the

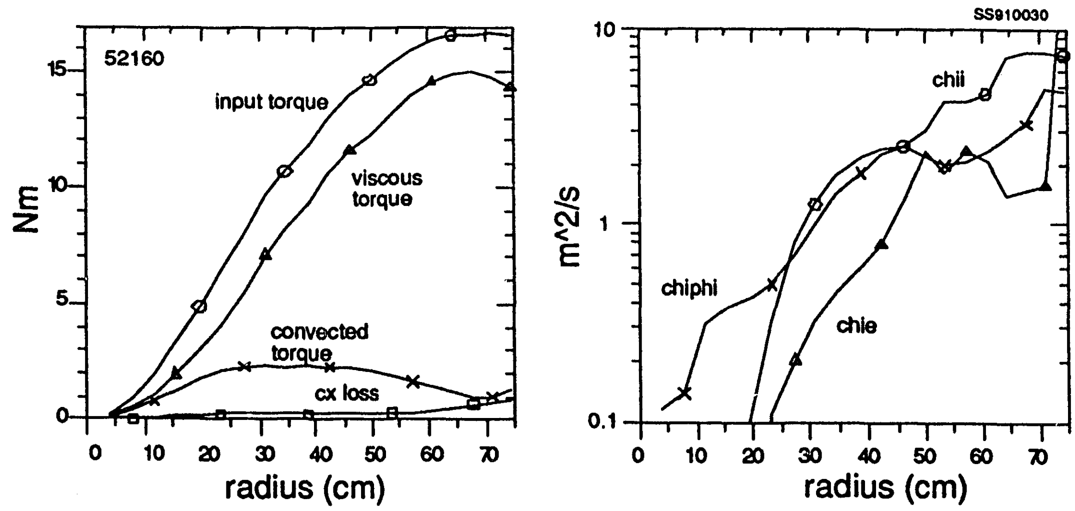

Figure 3: Momentum transport analysis for the plasma shown in Fig. 2.

beams and other heating sources. For a given, fixed $T_e(r)$ profile, we can compute a maximum allowable $T_i(r)$ by assuming that $\chi_i \equiv 0$, i.e. the ions do not transport *any* heat radially. Then, T_i will rise locally until the local heating rate from beams equals the power transfer to electrons ($q_{bi} + q_{bth} = q_{\text{conv-i}} - q_{ei}$). Similarly, we can compute a minimum allowable T_i by assuming that $\chi_e \equiv 0$, i.e. the *electrons* don't conduct any heat radially. At fixed T_e, this corresponds to decreasing the local T_i until all the power delivered to electrons is (locally) collisionally coupled to the ions ($q_{be}+q_{OH} = q_{\text{conv-e}}+q_{ei}$). Fig.4 illustrates the measured T_i and T_e in a typical beam-heated TFTR L-mode plasma (I_p = 1.2 MA, P_b = 17 MW) and the corresponding allowable minimum and maximum T_i. As is customary in L-mode plasmas [6], the standard steady-state power balance analysis indicates that the ions are responsible for most of the radial heat transport, and that they have a much larger thermal diffusivity than the electrons. But note that in the region $r \geq a/2$, the difference between $T_{\text{i-max}}$ and $T_{\text{i-min}}$ becomes quite small – so that an error of only ~1 keV in the measured temperature difference $T_i - T_e$ would cause us to conclude that the *electrons* are entirely responsible for the heat transport. Under these conditions, the measurement accuracy for T_e and T_i is not sufficient to determine which channel – ions or electrons – is primarily responsible for the radial heat flow. Because the electrons are an insignificant term in the *momentum* balance, we can still determine with good accuracy the transport rate for angular momentum in L-mode plasmas, and thereby infer the ion momentum diffusivity χ_ϕ.

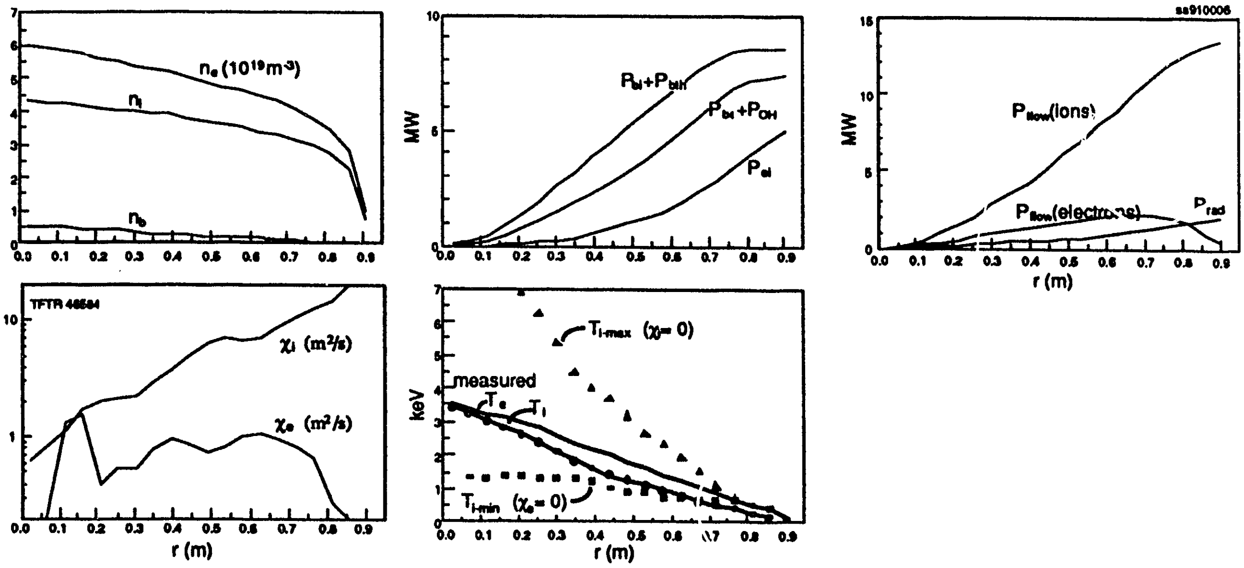

Figure 4: Standard power-balance analysis for a low-temperature TFTR L-mode plasma. (a) Density profile. (b) Calculated beam and ohmic power deposition to thermal ions and electrons. Note that roughly equal power is given to ions and electrons. However, because the electrons are hotter than the ions, about ~5 MW is given from the electrons to the ions. (c) Inferred heat flows in the ion and electron channel. The ions are inferred to carry most of the radial heat flow because they have the additional 5 MW from the electrons. (d) The inferred local ion and electron thermal diffusivities, χ_i and χ_e, deduced from the power flows in (c) and the measured temperature profiles. (e) The measured T_e and T_i profiles. The maximum and minimum ion temperatures consistent with classical ion-electron power coupling are also shown. Outside the plasma core ($r \geq a/2$), even small errors in the measured temperature difference $T_e - T_i$ would have a large effect on the electron-ion power coupling P_{ei}) term, and therefore also a large effect on the inferred profiles of χ_i and χ_e.

2. Deposition of torque by neutral beams

Neutral beams injected into a plasma follow a linear trajectory, along which they are attenuated through ionization and charge-exchange events with the plasma electrons and ions. This creates a population of energetic ions at the beam energy (and its half- and third-energy components), which then slows down in the plasma through Coulomb collisions with the thermal ions and electons, thereby depositing the beam power and momentum to the bulk plasma.

It is important to realize that most transport simulations deduce local transport coeffients by comparing the *measured* gradients (temperature, velocity) with *calculated* sources of heat and momentum from the beams. So the accuracy of the inferred χ_i, χ_e, and χ_ϕ depend as much on the accuracy of our calculations of the beam deposition and thermalization process as it does on accurate measurements of T_i, T_e, and v_ϕ.

The calculation of beam deposition process is very straightforward: the beam (usually represented as a large number of small collimated 'beamlets') is tracked along its linear trajectory through the plasma; in each spatial step ds a fraction of the beam $ds/\lambda_{\rm mfp}$ is deposited locally, where $ds/\lambda_{\rm mfp}$ is the mean-free--path against ionization and charge-exchange, which is calculated from known cross-sections and the local plasma density. The beam intensity is decremented by $ds/\lambda_{\rm mfp}$, then it proceeds on to the next spatial step, until the beam – normally attenuated by many e-folds in intensity – leaves the plasma.

- For rotating plasmas the beam energy must be evaluated in the frame of the rotating plasma when calculating $ds/\lambda_{\rm mfp}$, since all of the cross-sections depend on the relative energy of the beam neutral and the plasma particle. This can modestly increase the beam attenuation, as we will see later.

- The accuracy of the calculated deposition profile of beam neutrals as energetic ions depends largely on the accuracy of the atomic cross-sections. Park *et al.* [7] compared the rate of rise of electron density at the start of beam injection and found it to be in excellent agreement with the calculated deposition profile.

The next step is to follow the beam ions along their orbits, including Coulomb collisions with plasma ions and electrons, to determine where they deposit their energy, and to which species (electrons or ions).

- This can be done in a Monte-Carlo fashion, by numerically following the guiding-center orbits of an ensemble (typically 1000-4000) of beam ions. Collisions are included by scattering/slowing the ion at each step by an (random) amount commensurate with the local slowing-down and pitch-angle scattering times. For a description of a Monte Carlo treatment of beam deposition, see Hawryluk *et al.* [8].

- Alternately, one can solve the Fokker-Planck equation for the fast-ion population. The plasma is divided up into many radial zones, and the F.P. equation is solved separately in each of them. The inputs to the F.P. equation are the beam-ion 'birth' population as calculated by the neutral deposition code, and the local plasma parameters (n_e, T_e, T_i, Z_{eff}, etc.). The outputs are the power and momentum deposition rates to ions and electrons as a function of radius. See ~'allen [9] for a simple description of the Fokker-Planck equation and analytic approximations to its solution.

Although the Monte Carlo calculation is more comprehensive in that follows the expected guiding-center ion orbits (whereas the F.P. equation essentially presumes a zero banana width), *both calculational techniques assume that the beam ions are not subject to anomalous radial diffusion* as they slow down. This is quite a courageous assumption, since the final conclusion from most transport analyses is that the *thermal* plasma experiences very large rates of anomalous transport! Quite fortunately, for energetic ions, the assumption of no anomalous transport appears to be true. It has been tested in a variety of experiments [10–13]; the fast-ion diffusivity D_{fast} appears to be at least a factor ~10 less than the thermal transport rates – small enough so that the beam power should be deposited where the codes say it is.

Although there are no standard diagnostics which can measure the beam distribution function directly, there are two standard "consistency checks" which are routinely used to assess the validity of the Monte Carlo and Fokker Planck codes. These are:

- A comparison of the measured neutron emission with that calculated by the beam codes. For $D^o \rightarrow D^+$ injection, the neutrons are mostly made through collisions of beam ions with other beam ions or with thermal deuterons (i.e. the thermonuclear component from thermal-thermal fusion is small), so anomalous losses of the beam ions would show up as an overestimate of the measured neutron production.

- A comparison of the total stored energy, measured for example with a diamagnetic loop, with that calculated from integrating the measured density and temperature profiles and adding the calculated energy stored in the beam-ion population. This procedure is obviously a less sensitive test of classical beam-ion physics, since the beam stored energy typically represents only 10-50% of the total energy in a plasma.

2.1. The $\vec{J} \times \vec{B}$ torque

The deposition of beam torque differs from the deposition of beam power in one important way: torque can be coupled to the plasma directly through radial motion of the beam ions, i.e. no collisions required. Any radial motion of the beam ions represents a radial current, which when crossed with the poloidal magnetic field exerts a torque. Goldston[1] describes the physics clearly. Note that because F.P. codes assume a zero banana-width, they completely neglect the $\vec{J}_r \times \vec{B}_\theta$ torque (it isn't lost, it's collisionally deposited instead). Some illustrative cases are instructive:

- Consider a counter-injected ion born relatively near the outside of the plasma with a toroidal velocity $-v_{\phi-\mathrm{in}}$, with a pitch-angle such that it is banana--trapped on its first poloidal orbit. Assume it *leaves* the plasma on the co-going side of its first orbit (because its orbit-shift is outward) with a toroidal velocity $v_{\phi-\mathrm{out}}$. Clearly, the beam ion has imparted an angular momentum $-m_b R(v_{\phi-\mathrm{out}} + v_{\phi-\mathrm{in}})$ to the plasma, even though it was lost on its first orbit! This will be represented as a $\vec{J} \times \vec{B}$ torque in the orbit codes, because the beam ion effectively represents a large outward-directed $\vec{J}$.

  This process has practical implications: throughout the region near the plasma edge where counter-born beam ions are lost on their first orbit, there will be effectively no *power* deposition, but the deposition of beam momentum will be roughly *twice* the original beam momentum. Consequently, the profile of deposited torque can be much broader than that of power during counter-injection.

- When a beam ion becomes banana trapped, then its bounce-averaged rotation speed is zero (neglecting the precessional drift of the banana itself), and it effectively deposits all of its momentum to the plasma. This will show up in the beam-orbit codes as a $\vec{J} \times \vec{B}$ torque due to the orbit shift of the banana. Consequently, if the beams are injected quasi-perp so that many of them become banana-trapped early in their slowing-down lifetime, much of their torque will be deposited as $\vec{J} \times \vec{B}$ torque.

- For standard co-injected beam ions that don't banana trap, there is only a relatively small $\vec{J} \times \vec{B}$ torque due to the fact that the beam neutrals are typically born on the outside portion of their orbit (say at $R_o + r$) but their guiding-center orbit-averaged major radius is R_o. By μ conservation then, these ions' orbit-averaged $v_\parallel$ is less than their initial $v_\parallel$, and the difference is given to the plasma as $\vec{J} \times \vec{B}$ torque.

Illustrations of the $\vec{J} \times \vec{B}$ torque density for co-injection and counter-injection are shown in Figures 5 and 6.

2.2. *Collisional beam power and torque deposition*

The beam torque which isn't coupled to the plasma as $\vec{J} \times \vec{B}$ torque, and which isn't lost due to charge-exchange of the beam ion, is collisionally deposited to the

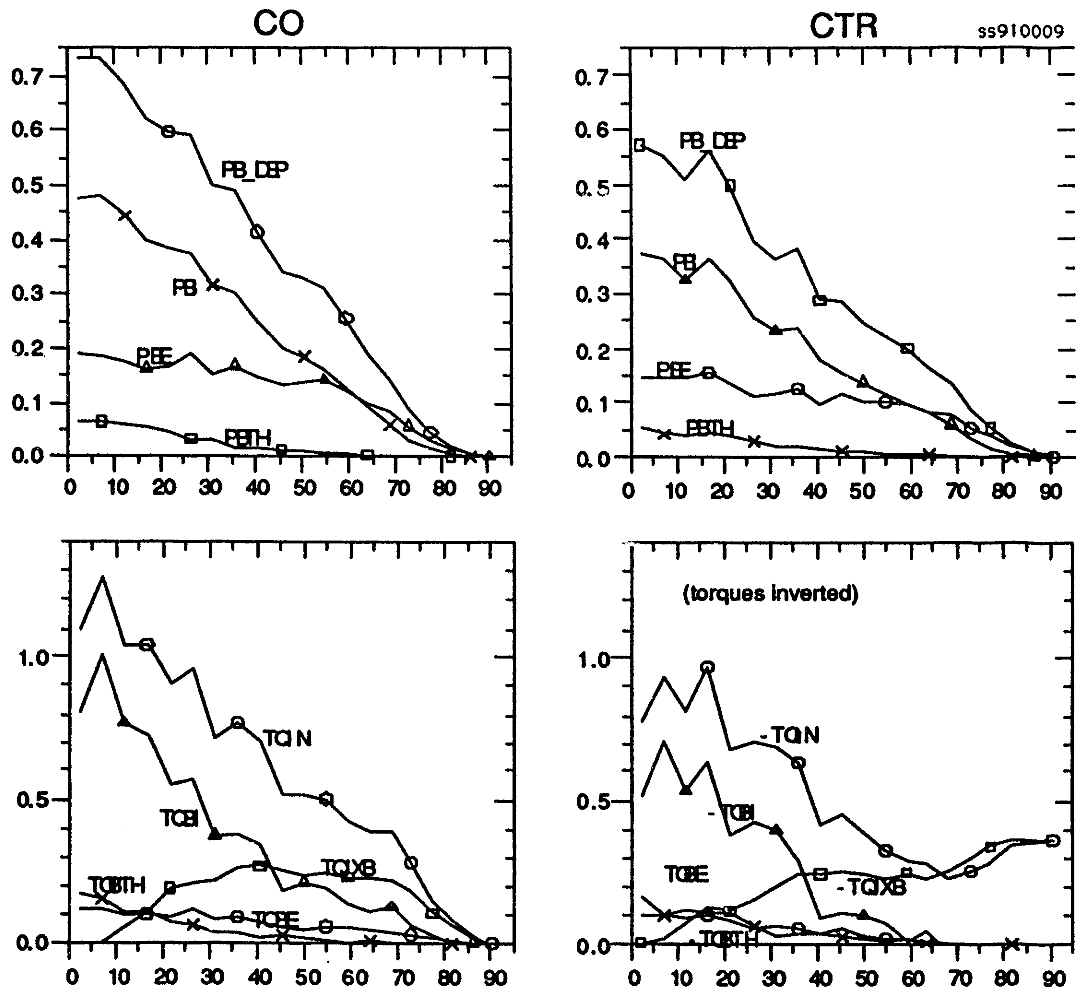

Figure 5: Comparison of calculated torque and deposition profiles for co- and counter-injection (the plasma conditions for the counter-injected calculation are the same as those for the co-injected plasma (see Fig. 8) except the direction of plasma rotation is reversed). Note the large contribution of $J \times B$ torque at the edge of the counter-injected plasma, which arises from beam ions which banana-trap on their first orbit & leave the plasma as co-going ions. These beam ions effectively deliver roughly twice their original angular momentum to the plasma edge as $J \times B$ torque.

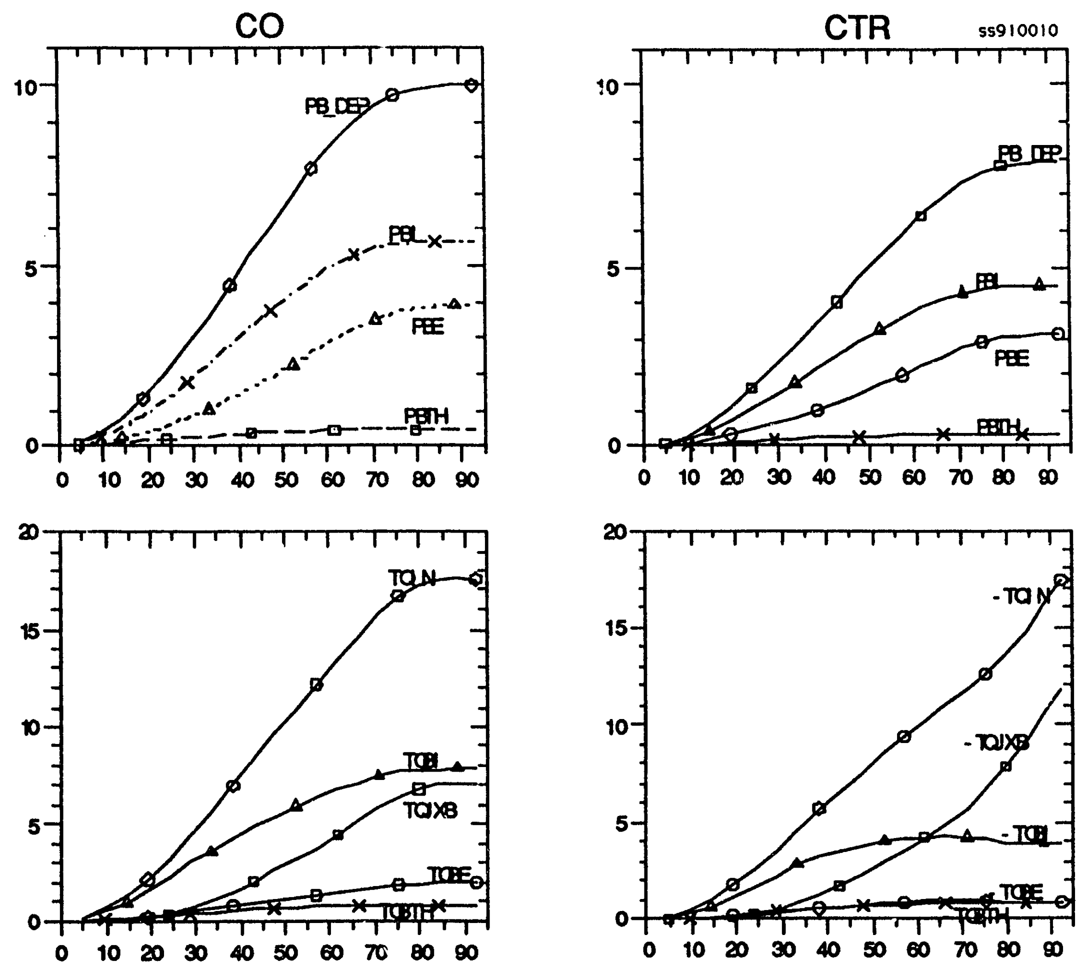

Figure 6: Comparison of integrated torque and deposition profiles for co- and counter-injection (using local deposition profiles shown in Fig. 5.

plasma electrons and ions. This section calculates the fraction of torque collisionally coupled to each species (electrons, ions, and impurities), and compares the result to the corresponding fractions for delivery of beam energy. There are two important results:

1. The (ions + impurities) get most of the beam power and torque in regions of high T_e, while the electrons get more in regions of low T_e. So in the center of most large experiments (JET, TFTR), the ions get most of the power, while in smaller devices (e.g. DITE, ISX-B) the electrons get most of the power.

2. The impurities get considerably more power and torque on a per-ion basis than do the hydrogenic ions. This can drive their temperature significantly higher than T_i of the hydrogenic ions under some circumstances.

Beam ions deposit their energy and momentum to the plasma electrons, ions, and impurities as a result of Coulomb collisions. To determine the fraction given to each, we must compute the rates at which the beam slows down on each species. The expressions below are direct evaluations of the formulae presented in the NRL plasma formulary [14] for the loss rate of beam energy and velocity to electrons (e), to a specific ion species (j), and to all of the ion species combined (i), e,g.

$$\begin{aligned} \left(\frac{dE_b}{dt}\right)_{\mathrm{b}\rightarrow\mathrm{species\,j}} &\equiv -E_b \nu_E^{b/j} \\ \left(\frac{d\vec{v}_b}{dt}\right)_{\mathrm{b}\rightarrow\mathrm{electrons}} &\equiv -\vec{v}_b \nu_s^{b/e} \end{aligned} \tag{2}$$

Note that the loss rate of velocity multiplied by the beam mass represents the rate of momentum transfer to each species. The units in the following expressions are: seconds, 10^{19} m^{-3}, keV, and amu.

$$\nu_E^{b/j} = \frac{854 n_j Z_j^2 \mu_b^{1/2} (\log \Lambda_j/15)}{E_b^{3/2} \mu_j} \tag{3}$$

$$\nu_E^{b/i} = \frac{854 n_e \mu_b^{1/2}}{E_b^{3/2}} \sum_j \frac{n_j Z_j^2}{n_e \mu_j} (\log \Lambda_j/15) \tag{4}$$

$$\nu_E^{b/e} = \frac{15.2 n_e (\log \Lambda_e/15)}{\mu_b T_e^{3/2}} \tag{5}$$

$$\nu_s^{b/j} = \frac{427(\frac{1}{\mu_j} + \frac{1}{\mu_b}) \mu_b^{1/2} n_j Z_j^2 (\log \Lambda_j/15)}{E_b^{3/2}} \tag{6}$$

$$\nu_s^{b/i} = \frac{427 \mu_b^{1/2}}{E_b^{3/2}} \sum_j n_j Z_j^2 (\log \Lambda_j/15) \left(\frac{1}{\mu_j} + \frac{1}{\mu_b}\right) \tag{7}$$

$$\nu_s^{b/e} = \frac{7.6 n_e (\log \Lambda_e/15)}{\mu_b T_e^{3/2}} \tag{8}$$

At high values of E_b, the beam energy and momentum is given primarily to electrons. At low E_b, the beam energy and momentum is given primarily to the thermal ions The beam energy transfer to ions and electrons is equal when $\nu_E^{b/i} = \nu_E^{b/e}$, and the beam momentum transfer to ions and electrons is equal when $\nu_s^{b/i} = \nu_s^{b/e}$. The equipartition point is reached at beam energies E_c for power and $E_{c\phi}$ for momentum, where

$$
\begin{aligned}
E_c &= 14.8\mu_b T_e (\sum_j \frac{n_j Z_j^2 \log \Lambda_e}{)}^{2/3} \\
E_{c\phi} &= 14.8\mu_b T_e (\sum_j \frac{n_j Z_j^2 (\frac{1}{\mu_j} + \frac{1}{\mu_b}) \log \Lambda_j}{n_e \log \Lambda_e})^{2/3}.
\end{aligned} \tag{9}
$$

From Eq. 9 it is a straightforward identity to show that in a deuterium plasma with a single, fully-stripped impurity (implying $\mu_j = 2Z_j$), $E_{c\phi}$ is just a factor $(Z_{\text{eff}}+1)^{2/3}$ larger than E_c. Figure 7 illustrates a typical numerical calculation of the torque deposition profile by the TRANSP code for co-injection. As expected, equal torque is delivered to electrons and ions at a lower electron temperature, only quite near the plasma edge, compared to the point of equal power sharing.

As shown in Fig. 8, the ratio of *total* torque collisionally coupled to ions vs electrons (4:1) is considerably greater than the corresponding ratio for power (1.5:1). Figure 8 also compares the shape of the torque deposition profile to the power deposition profile. The shapes of the power and torque deposition profiles are quite similar for co-injection, which is not surprising since they derive from the beam--ion population. There is less similarity for the deposition profile shapes during counter-injection due to a large contribution from the $\vec{J} \times \vec{B}$ torque, as discussed earlier.

Since the energy dependence of $\nu_E^{b/j}$ is independent of ion mass, the partition of the beam power and torque *among the ions* can be evaluated simply by comparing the damping rates at any energy for all of the ions. This yields

$$
\frac{q_{bj}}{q_{bi}} = \frac{n_j Z_j^2/\mu_j}{\sum_k n_k Z_k^2/\mu_k} \tag{10}
$$

$$
\frac{f_{bj}}{f_{bi}} = \frac{n_j Z_j^2(\frac{1}{\mu_j} + \frac{1}{\mu_b})}{\sum_k n_k Z_k^2(\frac{1}{\mu_k} + \frac{1}{\mu_b})} \tag{11}
$$

where q_{bj}/q_{bi} is the fraction of all beam power to ions which is given to the j^{th} ion species, and f_{bj}/f_{bi} is the fraction of all beam torque to ions which is given to the j^{th} ion species.

- Note that the beam interacts more strongly with the impurities than with the hydrogenic ions, due to the Z_j^2 dependence of the Coulomb cross-section. Consequently, the impurities receive a disproportionate share of the beam power and torque.

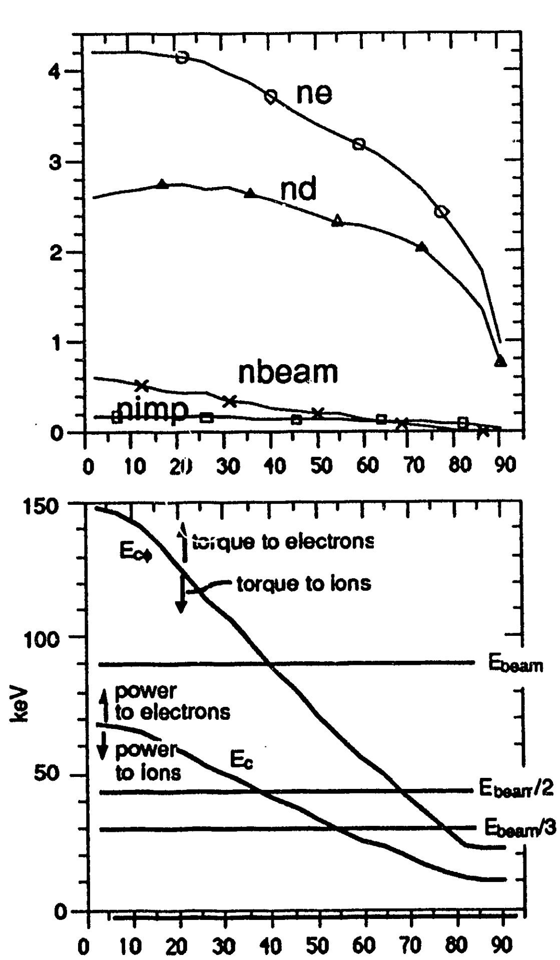

Figure 7: Numerical calculation of the torque deposition profile by the TRANSP code using a Monte Carlo orbit-following beam routine (2000 beam particles) to calculate the beam-ion orbits & their collisional torque deposition to thermal electrons and ions. Plasma conditions: (quasi-shot 41719) $R = 2.58$ m, $a = 0.93$ m, $I_p = 1.4$ MA, $B_t = 3.8$ T, $P_b = 11$ MW (co) $E_b = 90$ keV, $\overline{n}_e = 3.4 \times 10^{19}$ m^{-3}, $Z_{\rm eff} = 2.2$, $P_{ne} = 1.45$, and $\tau_E = 92$ ms $= 1.1 \times \tau_e^{\rm L-mode}$. Except at the plasma edge, all of the beam energies (full, half and third components) are less than $E_{c\phi}$, so the collisional beam torque is delivered mostly to the thermal ions rather than electrons.

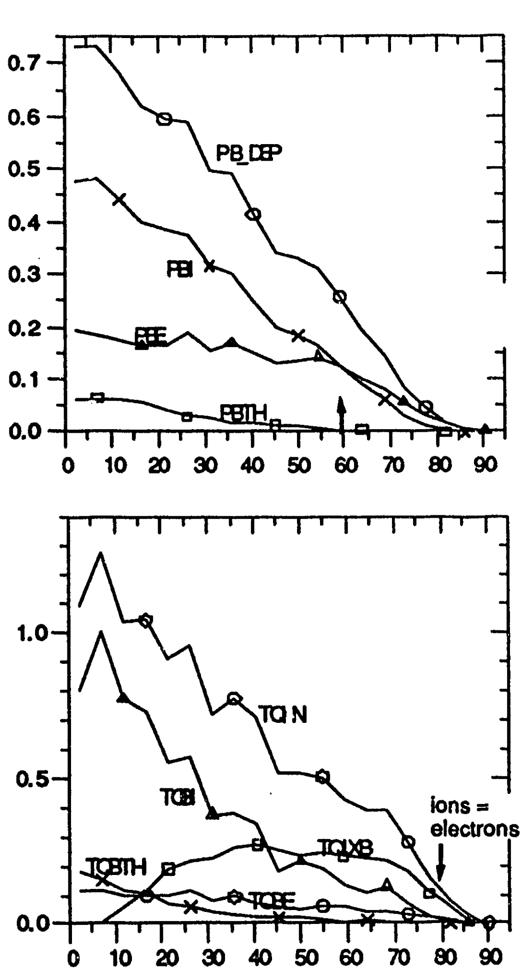

Figure 8: Power and torque deposition profiles as calculated by TRANSP for the plasma shown in Fig.7. The arrows in the left-hand plots show the radius at which equal beam torque (or power) is collisionally delivered to thermal ions and electrons.

The Z_j factor in the expression for *power* transfer to impurities is partially compensated by the additional factor $1/\mu_j$ (which for deuterium and fully-stripped impurities is $\approx 2Z_j$) – so the power delivered per ion is proportional to Z_j in a deuterium+ impurity plasma. This reflects the physics of scattering of fast, light particles by stationary, heavy ones: only a fraction $\sim \mu_{\text{light}}/\mu_{\text{heavy}}$ of the incident energy is transferred even in a head-on collision.

Below we evaluate the power and torque partition among the ion species for a typical hot-ion mode plasma. Although the impurities represent only ~8% of the ion density, they get about 1/3 of the beam power and 2/3 of the beam torque.

- Because the impurities get a disproportionate share of the beam power and an even larger fraction of the beam torque, they will become hotter, and rotate faster than the hydrogenic ions.

How much hotter and ***how much*** faster is an important issue for understanding plasma transport, because T_i and v_ϕ diagnostics typically measure the ***impurity*** temperature and rotation speed (either carbon through charge-exchange recombination spectroscopy or a metallic element through x-ray crystal spectroscopy), but we are more interested in the temperature and rotation speed of the hydrogenic ions.

Species	Z	A	n_j/n_e	percentage of all ions			
				density	mass	power	torque
D	1	2	0.646	91.8	64.6	64.7	32.3
C	6	12	0.057	8.1	34.2	34.2	59.9
Fe	26	56	0.0004	0.06	1.2	1.1	7.8

Table 1: Calculated partition of beam power and torque to various ion species for a deuterium plasma ($D^o \rightarrow D^+$) with carbon as the dominant light impurity and iron as a metallic impurity, assuming $Z_{\text{eff}} = 3.0$ and $Z_{\text{eff-metals}} = 0.3$.

We show below that there can be significant differences between the impurity and ion temperature in modest-density 'hot-ion mode' plasmas (the temperature differences are small in the L-mode regime). In both regimes the velocity differential among the ion species remains small, because momentum is rapidly exchanged among the ions. Actually, velocity equilibration is expected on more fundamental grounds: when v_ϕ of the hydrogenic ions becomes comparable to the sound speed, theory predicts that all ions should rotate at the same $\vec{E}_r \times \vec{B}_\theta$ speed [15].

2.3. *Calculation of ion-impurity T_i differential*

The temperature difference $T_j - T_h$ between the impurity and main hydrogenic ions will be limited by the power tranfser between them: As the impurity temperature rises above the hydrogenic T_h, the impurities will transfer energy to the main ions at a rate proportional to the temperature difference. The same is true for velocity. The local exchange rates of energy (q_{ij}) and momentum (f_{ij}) between two ion species (i and j) are

$$f_{ij} = \frac{1.08 n_i n_j Z_i Z_j (v_i - v_j)(\log\Lambda/15)}{T_i^{1.5}(\frac{1}{\mu_a} + \frac{1}{\mu_b})^{0.5}} \quad (12)$$

$$q_{ij} = \frac{1.62 n_i n_j Z_i^2 Z_j^2 (T_i - T_j)}{\mu_i \mu_j (\frac{T_i}{\mu_i} + \frac{T_j}{\mu_j})^{3/2}} \quad (13)$$

where the units of new quantities are f_{ij}= Nm^{-3}, $v = 10^5$m/s, and $q_{ij} = \mathrm{MW/m}^{-3}$. Similar to the expressions for beam power, the collision term for heat transfer is proportional to Z_j^2/μ_j while that for the momentum transfer is roughly proportional to Z_j^2 (the term $(1/\mu_j + 1/\mu_b)$ varies weakly with μ_j).

- Note that interspecies coupling of momentum is stronger than interspecies coupling of heat by roughly a factor Z_j.

In a nearly-pure plasma for which the hydrogenic ions still get most of the beam torque, the distribution of beam torque is also skewed in favor of the impurities by an additional factor of $\sim Z_j$, so we expect the fractional differences in rotation speed and temperature to be comparable. But even at modest impurity levels (see Table 1) the impurities get most of the beam torque – so the actual torque density delivered to the impurities doesn't increase as Z_j indefinitely, rather it saturates a the total torque available in the beam population.

- The net result is that under most conditions (Z_{eff} not terribly close to 1.0), friction among the ions will maintain their velocities closer together than their temperatures.

Not all of the power and torque delivered to an impurity species is available to 'support' its temperature above the hydrogenic ion temperature – some of it is lost radially through heat conduction. If we characterize the conducted heat as a local loss term $\propto \frac{3}{2} n_j T_j/\tau_{Ej}$, it is straightforward to calculate (algebraically) the distribution of ion temperatures and velocities among the various ion species that will result in a plasma once the source terms (beam power and torque) are specified. Typically one assumes that all of the ion species have the same local energy confinement time τ_{Ej}. A calculation for a hot-ion mode plasma under this assumption is shown in Fig. 9. The impurity temperature exceeds the deuterium temperature by $\geq 30\%$ at $r = a/3$. A similar calculation for the velocity shows at most a 7% difference in rotation speed between impurities and deuterium at the center.

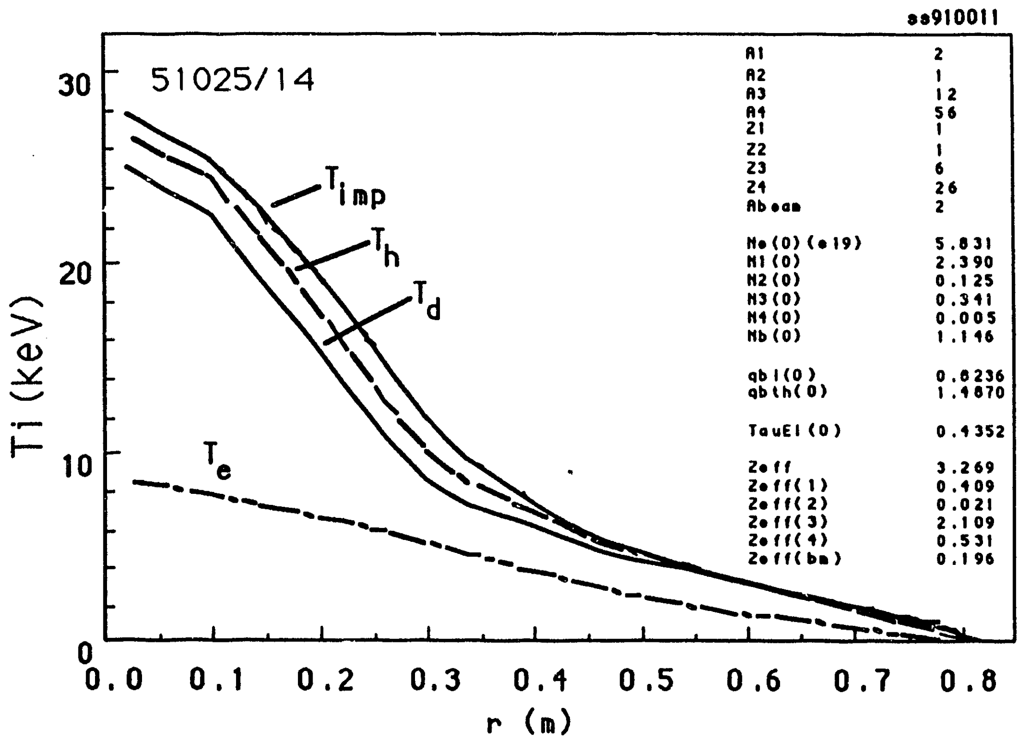

Figure 9: Calculated differences among the temperatures of four ion species (hydrogen, deuterium, carbon and iron) for the plasma shown in Fig. 7, assuming classical beam-ion and ion-ion power coupling for all species, and that all ion species have the same local energy confinement time.

2.4. Detour: thermalization torque in hot-ion mode plasmas

This section deals with a relatively obscure issue which can be safely skipped by the casual reader.

Typically, transport codes such as TRANSP numerically calculate the beam--ion distribution function down to $E = \frac{3}{2}T_i$, at which point the beam ions are considered to be "thermalized". These thermalizing beam ions represent a source of power (density) to the plasma, $q_{bth} = \frac{3}{2}T_i\dot{n}_{bth}$, where $\dot{n}_{bth}$ is the thermalization rate (m^{-3}/sec). Similarly, they deposit a thermalization torque to the plasma $T_{bth} = Rm_b\dot{n}_{bth}\langle v_{\phi-th}\rangle$, where $\langle v_{\phi-th}\rangle$ is the mean toroidal rotation speed of the beam-ion population at $E = \frac{3}{2}T_i$.

In most plasmas the beam-ion distribution is almost isotropic in the rotating plasma frame at $E = \frac{3}{2}T_i$, so $\langle v_{\phi-th}\rangle \approx v_\phi$, i.e. the mean beam rotation speed equals the local thermal rotation speed. The reason for this is simple: the beam ions' rate of pitch-angle scattering on thermal ions is $\sim Z_{\rm eff}$ times greater than their rate of slowing down on the thermal ions, so the beam ions isotropize before they thermalize.

However, in 'hot-ion' mode plasmas the ion temperature can reach a significant fraction of the beam energy, so the time required for beam-ion thermalization is short. This is particularly true in strongly rotating plasmas, for which the birth energy of the beam ions in the plasma frame can be ~half the beam energy in the lab frame. It is also particularly true for the fractional beam components ($E_b/2$, $E_b/3$) which are often born with *less* energy in the plasma frame than $\frac{3}{2}T_i$, i.e. they are considered to be "thermalized" instantaneously upon birth. Clearly, in these plasmas the beam-ion population is strongly anisotropic at $E = \frac{3}{2}T_i$, and so we expect $\langle v_{\phi-th}\rangle \gg v_\phi$.

- The arithmetic regarding the thermalization power and torque is correct even in the limit $\langle v_{\phi-th}\rangle \gg v_\phi$. However, regarding the beam ions as having "thermalized" at $E = \frac{3}{2}$ when they haven't yet *isotropized* introduces some errors into the calculation of the energy and momentum density of these ions.

Consider first the stored beam momentum. Since the beam ions are treated as part of the 'thermal' plasma when they reach $\frac{3}{2}T_i$, they are assigned the local rotation speed v_ϕ. But in fact they have on average a mean rotation speed $\langle v_{\phi-th}\rangle \gg v_\phi$, which will require a time $\tau_\perp$ to isotropize. Therefore, these "thermalized but not yet isotropized" (tbnyi) ions have an additional angular momentum density $\approx \dot{n}_{bth}m_bR\langle v_{\phi-th}\rangle\tau_\perp$ – which represents angular momentum of the thermal plasma – that is not normally included in transport analysis for χ_ϕ. Figure 10 illustrates a typical example for a strongly rotating, hot-ion mode plasma in TFTR. Due to the high temperatures, the beam thermalization term is the dominant source of beam torque at the plasma center (Fig. 10c), and the mean beam-ion velocity at time of thermalization is roughly twice the thermal rotation speed (Fig. 10e).

The angular momentum density of the tbnyi ions is about one-third of the thermal momentum density (Fig. 10h). Thus standard transport analsis, which neglects the contribution of the tbnyi ions, would underestimate the central momentum confinement by ~25%.

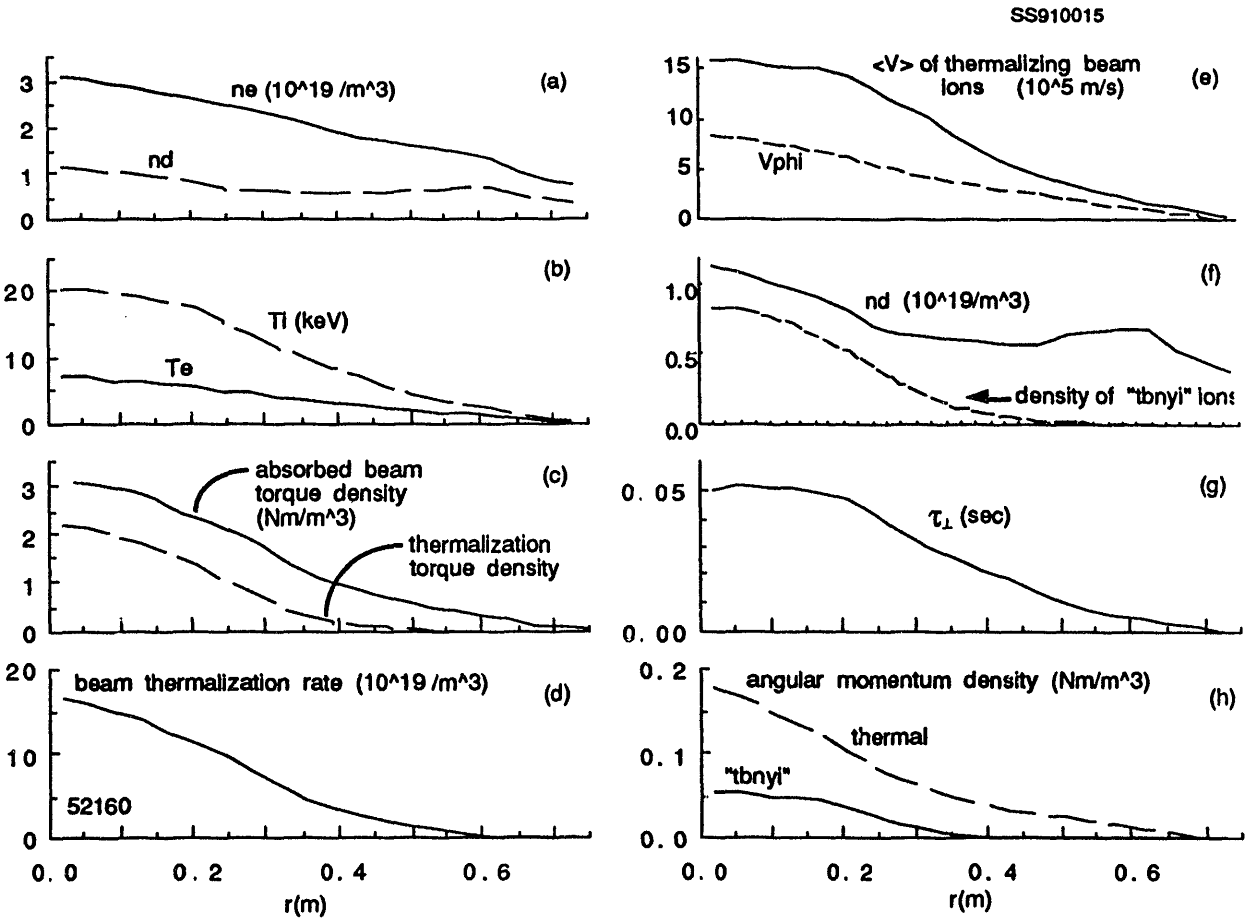

Figure 10: Calculation of angular momentum density of beam ions which reach $E = \frac{3}{2}T_i$ but which are not isotropized. The average toroidal speed of the thermalizing beam ions for this hot-ion mode shot is 15×10^5m/s, compared to the thermal rotation speed of 8×10^5m/s.

A corresponding error is introduced into the calculation of the energy density of the tbnyi ions. The standard assumption that the beam ions are isotopic at time of thermalization means that the energy of a just-thermalized beam ion is $\frac{3}{2}T_i + \frac{1}{2}m_b v_\phi^2$ in the lab frame, which may be less than their actual energy.

A larger casualty of our too-cavalier treatment of the thermalizing beam ions may be the calculation of beam-target neutron emission in strongly rotating plasmas, which is sensitive to the relative velocity of the high-energy beam icns and the target "thermal" deuterons.

3. Effects of Toroidal Rotation

There are several "classical" effects of strong toroidal rotation:

- In the rotating plasma frame, the beam energy is reduced, so the cross-sections for charge-exchange and ionization are increased. This leads to increased attenuation of beam neutrals, and less power deposited on-axis.
- Some of the beam power is deposited not as heating power, but as 'work' on the rotating fluid. This power is later returned as viscous heating, but typically at a larger radius.
- Lower birth energy of beam ions in the rotating plasma frame. This reduces their fusion reaction rate considerably, and also reduces the beam-driven current.
- Modification of impurity transport [16,17].
- Poloidal density asymmetries and modification of the plasma equilibrium driven by the centrifugal force [18–20].

There is also a growing theoretical literature on the possible effects of shear in the poloidal rotation speed (or radial electric field) on anomalous transport which will not be covered here. The paper by Biglari [21] is a reasonable starting point.

3.1. *beam deposition*

The mean free path of a beam neutral is given approximately by

$$\lambda_{mfp} = \frac{0.055 E_b}{A_b n_{e19}} \tag{14}$$

(meters, kev, amu, $10^{19}\mathrm{m}^{-3}$). Of course, since the attenuation takes place in the plasma, the beam energy must be evaluated in its frame of reference. In a plasma that is rotating strongly in the same direction as the beam injection, the beam energy in the plasma frame (E_{bpl}) can be considerably less than E_b in the lab frame:

$$E_{bpl} = E_b \sin^2(\theta) + \frac{1}{2} m_b (v_b \cos(\theta) - v_\phi(r)) \tag{15}$$

where θ is the angle between the neutral trajectory and the toroidal velocity v_ϕ, and v_b is the beam speed in the lab frame. A typical example is shown below in Table 2.

E_b	r/a	v_ϕ	E_{bpl}	$\frac{3}{2}T_i$
93.0	0.0	8.0	59.0	30
46.5	0.0	8.0	25.0	30
31.0	0.0	8.0	14.9	30
93.0	0.4	4.0	74.9	16
46.5	0.4	4.0	34.2	16
31.0	0.4	4.0	21.3	16

Table 2: Beam energy in the lab and rotating plasma frames for the three beam-energy components in a strongly rotating TFTR plasma (shot 52160) using quasi-tangential injection ($\cos(\theta) = 0.79$) and the measured ion temperature and rotation speed.

Note that at the plasma center, the half- and third-beam energy components are born with less than $\frac{3}{2}T_i$ in the rotating plasma frame, and thus actually *cool* the thermal ions!

According to Eq. 14 the total attenuation of the beam from the plasma edge to the center is roughly $I(r = 0)/I(r = a) = e^{-18.1\sqrt{2aR}\bar{n}_{e19}A_b/E_{bpl}}$, where I have assumed tangential beam injection so the path length from the edge to $r = 0$ is about $\sqrt{2aR}$. For the plasma shown in Table 2 the density was $\bar{n}_{e19} = 2.0$. The beam attenuation in a stationary plasma would be 1.54 e-folds. A mean rotation speed of 4×10^5m/s drops E_{bpl} to 74.9 keV and increases the attenuation to 1.91 e-folds, implying a ~30% reduction in central power deposition by the full-energy beam component (note that if one injected a *counter*-directed beam into this plasma, its energy in the plasma frame would be *bigger* than E_b, and it would experience *better* penetration to the plasma center).

Unless fully unbalanced beam injection into a low-density plasmas is employed on TFTR, the rotation speed is typically considerably less than the 8×10^5 m/s assumed in the previous calculation, and the expected effect on beam attenuation is correspondingly smaller.

3.2. beam 'work' on a rotating plasma and viscous heating

We saw in the previous section that, in the rotating plasma frame of reference, beam ions are born with less energy than in the lab frame. Consequently, in the rotating lab frame there is less beam power available to collisionally heat the thermal ions and electrons.

Where does the extra power go?

The answer is very simple: the beam ions exert a toroidal force $\vec{F}$ (per unit volume) on the rotating fluid – which is precisely the force needed to sustain the rotational velocity against viscous damping forces. We can calculate $\vec{F}$ from the usual Coulomb collisions between beam ions and the thermal electrons, and impurities. Since the plasma is moving, the toroidal beam force does 'work' on it at the rate $\vec{F} \cdot \vec{v}$ (per unit time and unit volume). The total power thus delivered as 'work' to the plasma over some volume is just the volume integral of all the $\vec{F} \cdot \vec{v}$ terms. Some of this power is converted to thermal energy by viscous heating ($q_{vis} = \sum_j m_j n_j \chi_\phi (\frac{\partial v_\phi}{\partial r})^2$), but the remainder flows out radially and is no longer available to heat the plasma inside the volume under consideration.

- The net result we expect toroidal rotation to broaden the beam power deposition profile, and can decrease the total power (collisional + viscous heating) delivered as well.

This section describes the arithmetic that is carried out by standard transport codes (TRANSP, SNAP, etc.) to calculate these effects. It pretty much follows Goldston's [1] derivation of the rotational energy balance, rewritten slightly to emphasize the radial energy flows induced by rotation. Stacey [22,23] has also evaluated the radial power flows associated with rotation.

Is this rotation-induced broadening of the power deposition profile large enough to seriously affect plasma heating? Energy confinement in hot-ion mode plasmas is indeed quite sensitive to the direction of injection (balanced *vs.* unbalanced), but the observed effects are considerably larger than we would attribute to the combined effects of rotation (including both the reduced beam penetration and the broadening of the deposition profile).

The absorbed beam power density in a rotating plasma, q_{abs}, is delivered to the plasma in the form of both heat and work:

$$q_{abs} = q_{be} + q_{bi} + q_{bth} + q_{bcx} + w_{(\vec{F}\cdot\vec{v})e} + w_{(\vec{F}\cdot\vec{v})i} + w_{(\vec{F}\cdot\vec{v})bth} + w_{(\vec{F}\cdot\vec{v})j\times B} \tag{16}$$

where q_{be} and q_{bi} are the collisional power delivered to thermal electrons and ions; q_{bth} is the power flow represented by thermalizing beam ions ($\equiv S_{bth}\frac{3}{2}T_i$), q_{bcx} is the power lost through charge-exchange of beam ions before they thermalize, and S_{bth} is the birth rate of thermalizing beam ions. The "w" terms represent "work" power densities done by the force of the slowing down beam ion population on the rotating plasma. The collisional force of the slowing down beam ions on the thermal electrons, acting on a plasma rotating with local velocity v_ϕ, gives rise to the first two work terms,

$$\begin{aligned} w_{(\vec{F}\cdot\vec{v})i} &= F_{bi\|}v_\phi \\ w_{(\vec{F}\cdot\vec{v})e} &= F_{be\|}v_\phi. \end{aligned} \tag{17}$$

Similarly, the total $\vec{j}_r \times \vec{B}_\theta$ force arising from radial motion of the beam ions yields a work term

$$w_{(\vec{F}\cdot\vec{v})j\times B} = (\vec{j}_r \times \vec{B}_\theta)v_\phi. \tag{18}$$

The thermalizing beam ions deposit momentum to the plasma at the rate $S_{bth}m_b v_{b\|}^{th}$, where $v_{b\|}^{th}$ is the average parallel velocity of the beam ions at time of thermalization. To evaluate the power terms arising from the thermalizing beam ions, they can be replaced by a thermalization force of the same magnitude ($F_{bth} \equiv S_{bth}m_b v_{b\|}^{th}$), *and* a source rate S_{bth} of zero-velocity ions. The thermalization force yields the usual work term $F_{bth}v_\phi$, while the zero-velocity particle source ***absorbs*** power at the rate $S_{bth}m_b v_\phi^2/2$ from the thermal plasma to provide energy for these ions to reach velocity equilibium. Thus the net work done by the thermalizing beam ions is

$$w_{(\vec{F}\cdot\vec{v})bth} = S_{bth}m_b v_\phi (v_{b\|} - \frac{v_\phi}{2}). \tag{19}$$

This definition of $w_{(\vec{F}\cdot\vec{v})bth}$includes the so-called "source-friction" term ($S_{bth}m_b v_\phi^2/2$) which is treated separately in reference [1].

The beam heating power delivered to the thermal plasma, which is available to sustain the temperature gradient against radial heat conduction, convection, radiation, charge-exchange, and ionization losses is

$$q_{heat} = q_{be} + q_{bi} + q_{bth} + q_{vis} \tag{20}$$

where q_{vis} is the heat generated through viscous damping of the plasma velocity, $q_{vis} = \sum_j m_j n_j \chi_\phi (\frac{\partial v_\phi}{\partial r})^2$, where the sum extend over all thermal ion species j.

- Note that the beam energy deposited in the form of work is not available as heating power. Most of it is eventually converted to viscous heating power, but at a larger minor radius than where it was originally deposited.

As we shall see, there is a radial flow of energy driven by rotation which (along with a few other terms) at any radius is equal to the integrated $\vec{F}\cdot\vec{v}$ work done by the beams minus the total work energy that has been converted into heat through viscous dissipation.

At steady state, Goldston's Eq. 23 [1] for the balance of rotational energy integrated out to an arbitrary minor radius r is

$$\begin{aligned}
\int_0^r q_{vis}\, dV \;=\; & \int_0^r dV\, (w_{(\vec{F}\cdot\vec{v})e} + w_{(\vec{F}\cdot\vec{v})i} + w_{(\vec{F}\cdot\vec{v})bth} + w_{(\vec{F}\cdot\vec{v})j\times B} + w_{(\vec{F}\cdot\vec{v})ioniz}) \\
& - \int_0^r dV\, \frac{\sum_j n_j m_j v_\phi^2}{\tau_{\phi cx}} \\
& + A_r v_\phi (\sum_j m_j n_j)\chi_\phi \frac{\partial v_\phi}{\partial r} - A_r \sum_j m_j (\vec{\Gamma_j}\cdot\hat{r})\frac{v_\phi^2}{2}
\end{aligned} \tag{21}$$

where Γ_j is the radial flux of the jth ion species, $dV = 4\pi^2 Rr dr$ for circular concentric flux surfaces, and A_r is the surface area of the flux surface ($A_r = 2\pi^2 Rr^2$ for circular concentric flux surfaces), and $w_{(\vec{F}\cdot\vec{v})ioniz}$ is an additional work term arising from creation of new plasma ions through ionization of multiple ion species j at rates S_j, at mean birth velocities $v^b_{\|j}$:

$$w_{(\vec{F}\cdot\vec{v})ioniz} = \sum_j S_j m_j v_\phi (v^b_{\|j} - \frac{v_\phi}{2}). \tag{22}$$

We can substitute this expression for q_{vis} into Eq. 20 to calculate how much rotation reduces the power available for heating;

$$\begin{aligned}\int_0^r q_{heat}\, dV \;\; &= \;\; \int_0^r dV\,(q_{abs} - q_{tcx}) \qquad \leftarrow \text{usual terms} \\ &+A_r v_\phi (\sum_j m_j n_j)\chi_\phi \frac{\partial v_\phi}{\partial r} - A_r \sum_j m_j(\vec{\Gamma}_j \cdot \hat{r})\frac{v_\phi^2}{2} \quad \leftarrow \text{rotation terms} \\ &+ \int_0^r dV\,(w_{(\vec{F}\cdot\vec{v})ioniz} - \frac{\sum_j n_j m_j v_\phi^2}{\tau_{\phi cx}}) \qquad \leftarrow \text{usually small terms}\end{aligned} \tag{23}$$

Here q_{abs} is the density of *absorbed* beam power, calculated by a neutral beam attenuation/deposition code (which includes the effect that plasma rotation reduces the relative beam-target energies and therefore decreases beam penetration).

The first term on the right-hand-side represents the total power inside the radius r available to heat (and push) the plasma. The next two terms (second line) represent radial flows of energy driven by rotation; the former represents the work done by the rotating plasma against the restraining viscous force ($F_{vis} \equiv \sum_j n_j m_j \chi_\phi \frac{\partial v_\phi}{\partial r}$) at a flux surface of radius r (which is where all of the variables in these two expressions are evaluated), and the latter term represents a radial convection of rotational energy. The last two terms (third line), which are typically small in the plasma interior, represent the rotational energy lost to charge-exchange, and the work that needs to be invested to bring newborn ions up to the local rotation speed.

3.3. sample calculation

Figure 11 illustrates these power flows as calculated by SNAP for the nominal plasma conditions of shot 35782, assuming a velocity profile of the form $v_\phi(r) = 8 \times 10^5(1 - (\frac{r}{a})^2)^3$ m/sec, and a $\chi_\phi(r)$ consistent with the calculated beam torque and this velocity. The distribution of beam power to thermal heating, work against the moving plasma, and charge-exchange losses is illustrated. Fig. 12 shows the power delivered to the *thermal* plasma, which naturally excludes the work terms but includes the viscous heating. As we expected, the profile of rotational work done by the beam ions is much more peaked than the viscous heating (which must

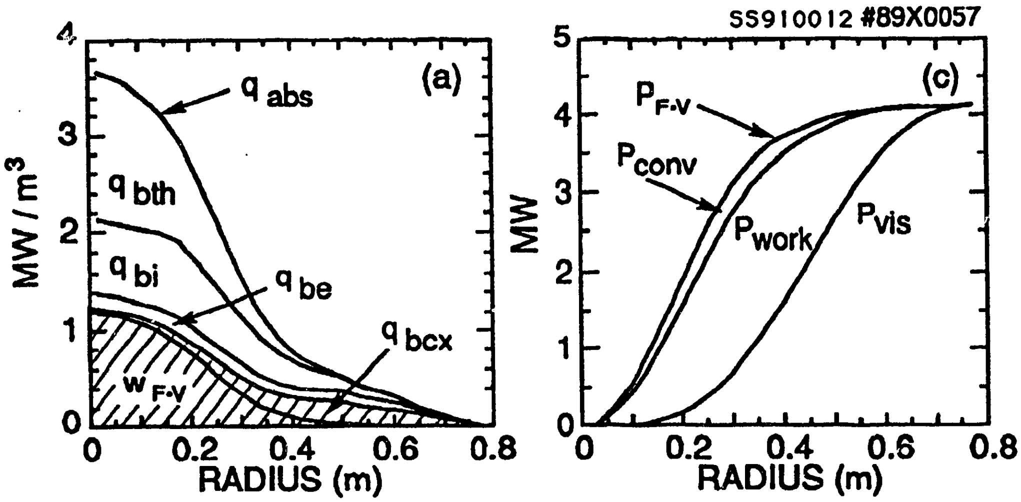

Figure 11: (a) Calculated beam power deposited as 'work' (shaded region) on a plasma rotating with a central velocity of 9×10^5 m/s, compared to the beam power collisionally coupled to thermal ions and electrons. (c) Corresponding volume--integrated power flows. $P_{F.V}$ is the power invested by the beams as work against the rotating fluid plasma. Some of this power,P_{vis}, is recouped as local heating via viscous dissipation, but the difference ($P_{F.V} - P_{vis}$) represents the beam power that is not available for heating.

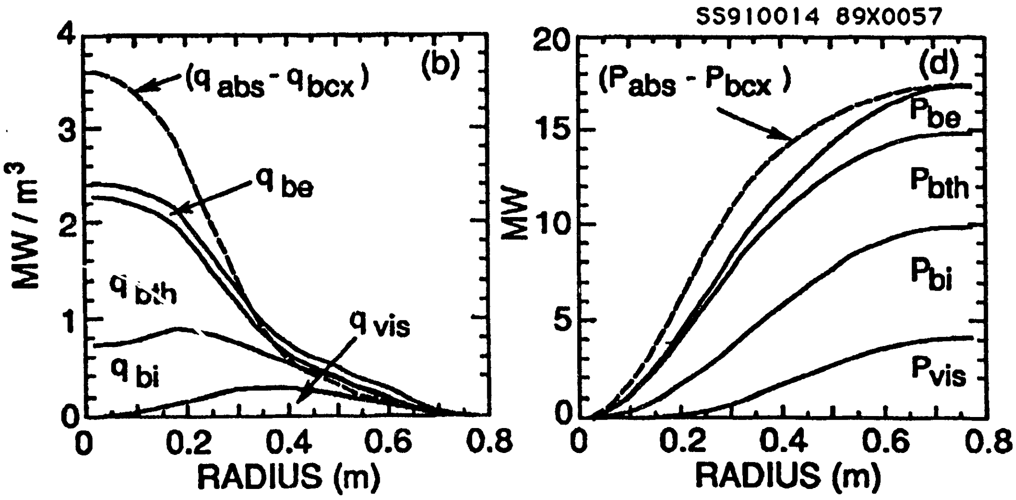

Figure 12: (b) Local heating rates corresponding to the calculations in Fig.11. In the absence of rotation, the collisional and beam thermalization terms ($q_{be}+q_{bi}+q_{bth}$) would sum to the available beam power density ($q_{abs} - q_{bcx}$) of 3.6 MW/m^3 at the plasma center. Rotation reduces this thermal heating to only 2.4 MW/m^3 at the center. The missing power is returned to the plasma as viscous heating at larger minor radius. (d) Corresponding integrated power deposition profiles. Overall, the effect of rotation is to convert ~4 MW of centrally-deposited beam power to ~4 MW of viscous heating.

vanish at the magnetic axis because $\frac{\partial v_\phi}{\partial r} = 0$ at $r = 0$), thus, the rotation broadens the delivered power profile. Fig. 11c shows the rotational energy balance Eq. 21; the integrated rotational work done by the beams out to any minor radius r is equal to the viscous heating within that volume, plus the rotational energy convected across the flux surface, plus the work done by the plasma against the restraining viscous force acting across the flux surface. Charge-exchange transport of rotational energy is typically calculated to be negligible for all rotating TFTR discharges, because the charge -exchange times are long in the plasma center, while nearer the edge the rotational energy is small ($(v_\phi/v_{th})^2 << 1$)).

In this particular case, the plasma recovers as viscous heating *all* of the beam power deposited as work, because our assumption of a parabolic-cubed velocity profile implies that both the convection term and the surface work term vanish at the plasma edge ($v_\phi = 0$ at $r = a$). Thus, in this case the only effect of rotation is to broaden the profile of delivered thermal power, and thereby to reduce (modestly, as we shall see) its heating effectiveness. In the more general case where neither v_ϕ nor $\frac{\partial v_\phi}{\partial r}$ vanishes at the plasma edge, the rotational energy flows at the plasma edge are also nonzero, and therefore directly reduce the total integrated heating power and τ_E. The integrated power delivered to the thermal plasma is shown in Fig. 12d. Notice that viscous heating accounts for roughly 25% of the total.

3.4. *Effect of rotation on beam ion population*

In the sections above we have seen that strong plasma rotation can produce a modest increase in beam attenuation and a modest broadening of the beam power delivered to the thermal plasma. A far stronger effect is on the beam ion population itself: because the beam energy is reduced in the plasma frame, both the beam-target and the beam-beam fusion reactivity are decreased significantly. For example, Hendel [24] calculated that stopping the rotation in a co–injection plasma with $v_\phi(0) = 5.2 \times 10^5$ m/s would increase the beam-target neutron rate by 65% and the beam-beam rate by a factor of 4, mostly due to the increassed slowing down time when rotation $\approx$0.

The toroidal beam-driven current (due to the circulating beam-ion population) is reduced by rotation for the same reason: it reduces the beam energy in the plasma frame, increases the drag, and thereby decreases the fast-ion population. Zarnstorff has calculated that the beam-driven (including a modest bootstrap contribution) could be increased from ~1 MA to ~1.7 MA if the associated plasma rotation could be stopped, for example using RF heating.

3.5. Effect of Heating Profile Modifications on τ_E

Experimentally, the energy confinement time τ_E^{dia} measured with a diamagnetic loop shows a strong correlation with the beam balance parameter $B \equiv (P_{co} - P_{ctr})/(P_{co} + P_{ctr})$ [25] which in turn is strongly correlated with the rotation speed. The maximum τ_E^{dia}decreases from 170 msec with balanced injection to about 105 msec with pure co-injection. Can this difference be attributed entirely to the classical effects of a increased beam attenuation and a broadened power deposition profile, or does the heat conductivity change?

We will use the "heating effectiveness" parameter developed by Callen et al. [26] to estimate the variations in stored plasma energy brought about by changes in the heating profile, assuming *fixed* profiles of ion and electron thermal diffusivity, χ_i and χ_e. Callen represents global energy confinement time τ_E as the product of an "ideal" confinement time τ_χ (which is independent of the heating profile) and the heating effectiveness, η, which is calculated from a radial integral of the heating profile and other quantities.

To evaluate η, we performed a steady-state power balance for discharge 35782 using the SNAP code, to determine the radial profiles of χ_e and χ_i that are consistent with the measured profiles of $T_e(r)$, $T_i(r)$, and $n_e(r)$. In this analysis the convective heat fluxes ($q_e = \frac{3}{2} - \frac{5}{2} \times T_e\Gamma_e$ and $q_i = \frac{3}{2} - \frac{5}{2} \times T_i\Gamma_i$) which dominate the power balance near the plasma center in TFTR supershots [27,28] were turned off, so that the calculated χ_i and χ_e are consistent with the *total* power fluxes (convective plus conductive) throughout the plasma. The heating effectiveness η was then calculated using the $n_e(r)$ and $\chi_e(r)$ from the SNAP analysis in the appropriate heating-effectiveness equations, Callen's Eqs 22-24. A ad-hoc correction (which ultimately amounted to only 12%) was used to extend Callen's expressions to the case for which $T_i \neq T_e$. Then the heating effectiveness was determined for other plasma conditions by re-calculating the heating profile (including the effects of rotation, broader beam deposition profile arising from higher $\overline{n}_e$, etc.) and then re-evaluating the integrals for η, using the previously determined profiles of $\chi_i(r)$ and $\chi_e(r)$. To evaluate the rotational power flows for each case, which requires knowledge of $v_\phi(r)$ and $\chi_\phi(r)$, SNAP determined the radial profile of $\chi_\phi(r)$ which was consistent with its calculation of the beam torque deposition profile and an assumed velocity profile.

- A modest reduction of 11% in τ_E is projected for the nominal plasma conditions ($\overline{n}_e = 3.9 \times 10^{19}$ m^{-3}, parabolic-cubed velocity profile) if the plasma rotates at a speed of 8×10^5 m/sec.

(Recall that τ_E is observed to decrease by $\sim$ 38% as one progresses from balanced to pure co-injection). A considerably larger reduction in τ_E(25%) is calculated for broader velocity profiles (parabolic), which however have not been observed in TFTR in modest-current, conditioned discharges. Based on the observed scaling of rotation speed in TFTR, $v_\phi(0) \propto \Gamma_b/\overline{n}_e$ [29,30], we would expect a rotation speed

$v_\phi(0) \sim 8 \times 10^5$ m/sec for *co-tangential* injection of 22 MW at the observed $\overline{n}_e$. However, the beam sources on TFTR are equally divided between co- and counter-injection, with a maximum available unidirectional power of about 15 MW; at $P_b = 22$ MW there can be at most 7 MW of unbalanced power and correspondingly smaller rotation speed (the actual $v_\phi(0)$ for shot 35782 was 1.5×10^5 m/sec).

Parameter	Range	$\overline{n}_e$	$S_{tot}(0)$	$n_e(0)$	P_n	$H(0)$	τ_E	$\tau_E(rot)$
v_0 −(3)	0 →9	3.9	3.40 →3.07	8.16 →8.02	3.11 →3.05	6.72 →3.98	122 →108	122 →120 →123
v_0 −(3)	0 →9	6.2	2.31 →1.81	6.69 →6.23	2.79 →2.63	4.34 →2.30	111 →99	111 →109 →122
v_0 −(1)	0 →9	3.9	3.40 →2.86	8.16 →7.74	3.11 →2.97	6.72 →3.89	122 →92	122 →113 →120.

Table 3: Summary of density and energy confinement simulations. Nominal plasma had $\overline{n}_e = 3.90 \times 10^{19}$ m^{-3}, $E_b = 108.5$ keV, Shafranov shift = 21.7 cm, $v_\phi(0) \leq 1.5 \times 10^5$ m/s. Units: $\overline{n}_e$and $n_e(0)$ in 10^{19} m^{-3}; S_{tot} in 10^{20} m^{-3}/sec; v_ϕ in 10^5 m/sec; $\tau_E$and $\tau_E(rot)$ in msec. The (3) and (1) identifiers listed for the velocity represent parabolic-cubed and parabolic velocity profiles, respectively. The dependent quantities (S_{tot}, $n_e(0)$, P_n, $H(0)$, τ_E, and $\tau_e(rot)$) generally changed monotonically with velocity, One exception was the energy confinement time including stored rotational energy, $\tau_E(rot)$, which first decreased with increasing plasma velocity, reached a minimum, and then increased once again for central velocities in excess of 5×10^5 m/s.

4. Experimental Observations

4.1. *Is momentum transport diffusive?*

Most analyses of momentum transport assume that the radial flux of toroidal momentum is driven by

- a diffusive, viscous term of the form $R^2 n_j m_j \chi_{\phi j} \frac{\partial \omega_{\phi i}}{\partial r}$, and
- a convective term arising from particle transport of the form $R^2 m_j \Gamma_j \omega_{\phi j}$ (which is usually small).

However, there may be other terms such as

- off-diagonal terms such as $R^2 n_j m_j \chi_{tj} \frac{\partial T_i}{\partial r}$, i.e. momentum flux driven by a temperature gradient;
- pinch terms of the form $R^2 n_j m_j \omega_{\phi j} v_{\rm pinch}$;
- and nonlinear terms of the form $R^2 n_j m_j \chi_{\phi \rm nl} (\frac{\partial \omega_{\phi i}}{\partial r})^n$ with $n \neq 1$.

There is very little experimental data that validates or rejects the existence of these 'other' terms which might drive radial flows of angular momentum. Since the functional form of $\chi_\phi(r)$ is unknown, it is difficult to distinguish the effects of say a nonlinear term from a complicated dependence of χ_ϕ on local parameters. Some progress has been made with respect to the momentum pinch: one can look for a momentum pinch by aiming a neutral beam so that it misses the magnetic axis, thereby creating a region in the plasma core with no momentum input. A significant inward-directed momentum pinch would manifest itself by peaking the velocity in the core, whereas simple diffusion would predict a flat velocity profile inside any region with no momemtum sources. Such an experiment cannot easily identify an ***outward*** momentum pinch, since it would be difficult to distinguish it against arbitrary forms of $\chi_\phi(r)$.

Figure 13 illustrates the evolution of the velocity profile measured by charge--exchange recombination spectroscopy during edge-heating in TFTR [31–33,10]. A single neutral beam source with $P_b = 2.0$ MW was injected into an $r/a = 2.36/0.71$ m plasma in the horizontal midplane from 4.0 - 4.5 seconds at a tangency radius of 2.84 m. The calculated torque deposition profile was essentially zero inside $r \leq 0.3$ m, and peaked at $r \approx 0.48$ m.

- Note that the velocity profile shows no evidence of peaking inside the region where there is no beam torque. Thus, qualitatively, there is no evidence for an inward-directed momentum pinch.

As discussed below, the time history of $\omega_\phi(r,t)$ can be reproduced quite well by the standard momentum diffusion equation without a momentum pinch term.

The discharge was analyzed with the TRANSP code to deduce the time evolution of $\chi_\phi(r,t)$ from the measured $v_\phi(r,t)$ and the calculated torque deposition profile, assuming no pinch term. The inferred $\chi_\phi(r,t)$ was then smoothed in time (30 ms), clipped with a minimum of 0.1 m^2/s and a maximum of 50 m^2/s, and then used as the ***input*** to a velocity simulation code which solves the momentum balance equation using the measured density and the calculated torque profiles to ***predict*** the time history of $\omega_\phi(r,t)$. The simulation does not include a pinch term. As shown in Fig. 13, the simulation reproduces the measured time evolution of ω quite well.

A similar experiment had been carried out previously by modulating the edge-heating beam in three 100 ms pulses separated by 100 ms off-periods [34]. As shown in Fig. 14, the measured central velocity was also modulated in time, but with a phase lag. The time history of $v_\phi(0)$ could be reproduced quite well assuming a flat $\chi_\phi(r) = 3.0\text{m}^2/\text{s}$, or a radially-dependent $\chi_\phi(r) = 1.4(1+2\frac{r}{a})\text{m}^2/\text{s}$, and no momentum pinch. Similar analyses for central-heating required a larger χ_ϕ by about a factor of two. These edge-heating results do not necessarily rule out a momentum pinch, since the edge velocity wasn't measured (so it isn't known if

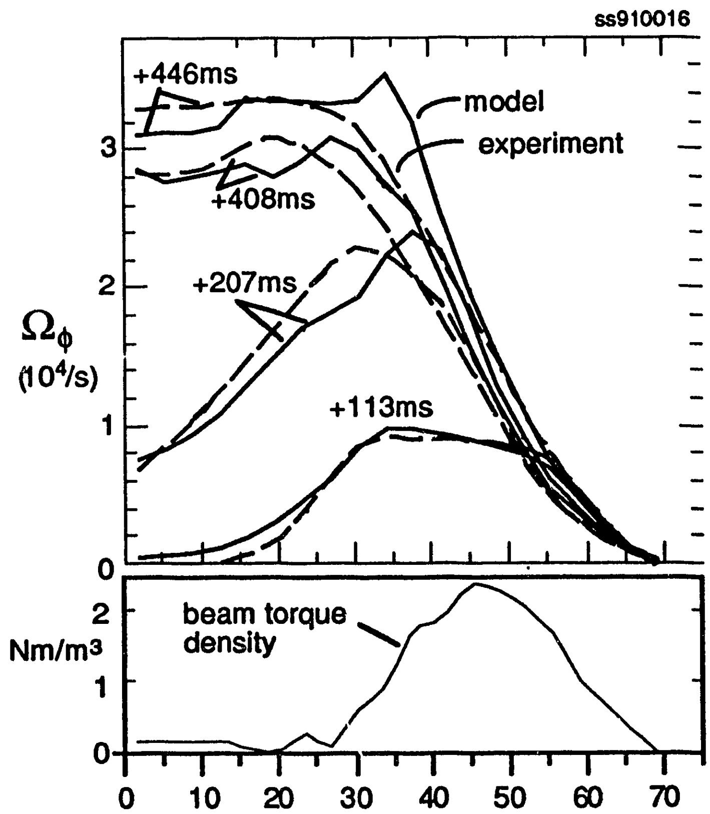

Figure 13: Measured time evolution of toroidal angular rotation frequency during edge-heating compared to a simulation with zero momentum pinch.

the velocity gradient was zero inside the region of zero torque), but if one were present, we might have expected the inferred χ_ϕ to be larger during edge-heating then during central-heating. The observation of a significant rotation speed during edge-heating *does* imply a significant level of diffusive-driven momentum transport. If 'local' damping mechanisms such as charge-exchange or ripple were the dominant momentum loss process in these plasmas, the center would not have accelerated to nearly 2/3 the rotation speed obtained during central-heating.

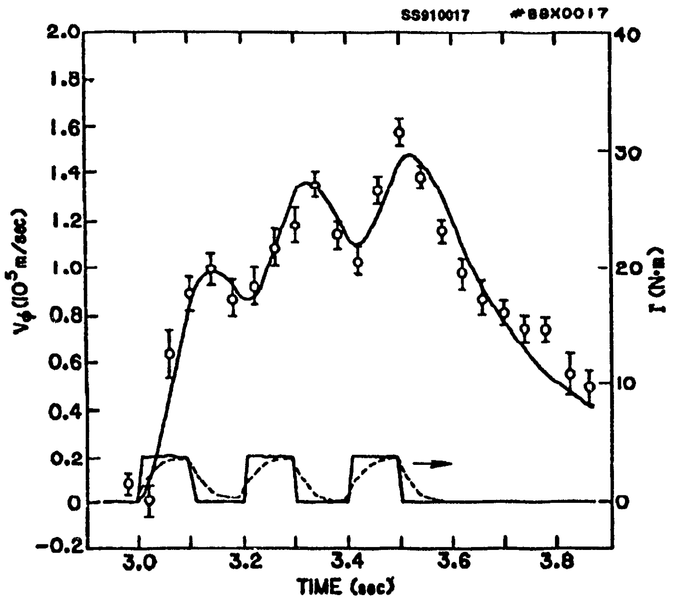

Figure 14: Measured central rotation speed during modulated edge heating. The solid line is a simulation based on $\chi_\phi(r) = 3.0$ m^2/s with no momentum pinch.

4.2. *Measurements of global and local momentum transport.*

The next few figures summarize the scaling results of central rotation speed with input torque from a number of tokamaks. PLT, TFTR, and DIII-D all observe a roughly linear increase of $v_\phi(0)$ with input torque, while ASDEX found it to scale with input torque as $\propto T^0.6$. In ISX-B (not shown) the central rotation speed saturated relatively quickly with beam power.

Next we present several analyses of local momentum transport from TFTR in the supershot regime, another from ASDEX in a variety of confinement regimes, and from JET in the hot-ion H-mode. An interesting correlation between $T_i(0)$ and $v_\phi(0)$ observed in the JT-60 hot-ion mode is illustrated in Fig. 23. For both TFTR and ASDEX, it is observed that the region where χ_ϕ experiences the largest improvement (relative to L-mode values) is also the region where the density gradient is the steepest. In the ASDEX H-mode the largest change in χ_ϕ occurs at the plasma edge, which corresponds to the region of large ∇n_e, although χ_ϕ is lower throughout the plasma. Measurements of the radial space potential from ISX-B (Fig.22) during ohmic, co-, counter-, and balanced injection are in qualitative agreement with predictions from the force balance.

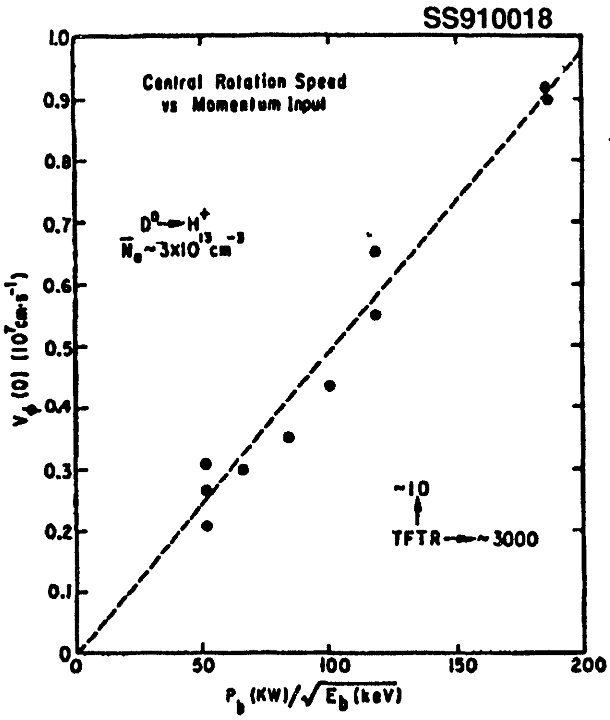

Figure 15: Measured central rotation speeds in PLT as measured from Doppler shifts of the FE XX line[35] for $D^o \rightarrow H^+$ beam injection. The extrapolation to TFTR with ~32 MW was remarkably accurate.

Acknowledgements

This work was supported by the U.S. DOE contract number DE-AC02-76-CHO-3073.

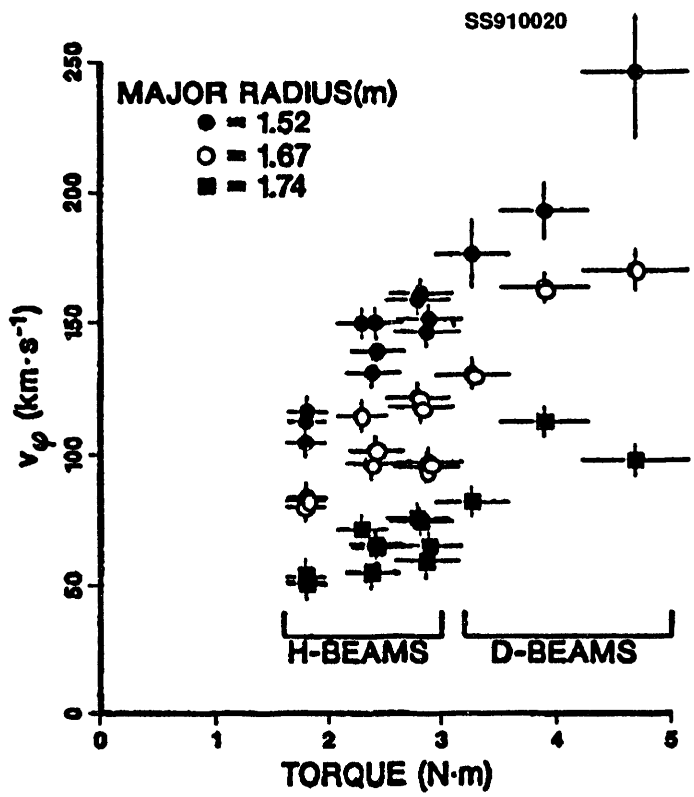

Figure 16: Toroidal rotation velocities as measured by CXR in the Doublet III tokamak (divertor plasmas) at three different major radii versus input beam torque [36]. Plasma conditions were I_p = 700 KA, B_t = 2.5 T and $\overline{n}_e = 8 \times 10^{19}\mathrm{m}^{-3}$. The central rotation speed rises linearly with input torque, but the rotation speed further out increases less rapidly.

Figure 17: (a) Central rotation speeds in TFTR plasmas measured by x-ray crystal spectroscopy as a function of beam force per particle [37]. The dependence of central rotation speed on I_p is weak. (b) Comparison of central rotation speed scaling in TFTR reduced-bore plasmas ($R/a = 3.00/0.60$) with the PLT results at the same I_p, showing a considerable size scaling of momentum transport.

Figure 18: Comparison of local momentum transport in regimes of standard versus 'improved' confinement in ASDEX [38]. Similar to the TFTR 'supershot' regime with a centrally peaked density profile (Fig. 19), the peaked-density regimes on ASDEX (pellet and counter-injection) show the largest improvement in χ_ϕ in the plasma core, where ∇n_e is most affected. The improvement in $\chi_\phi$in H-mode plasmas occurs mostly at the plasma edge, which is also where the largest change in ∇n_e is observed.

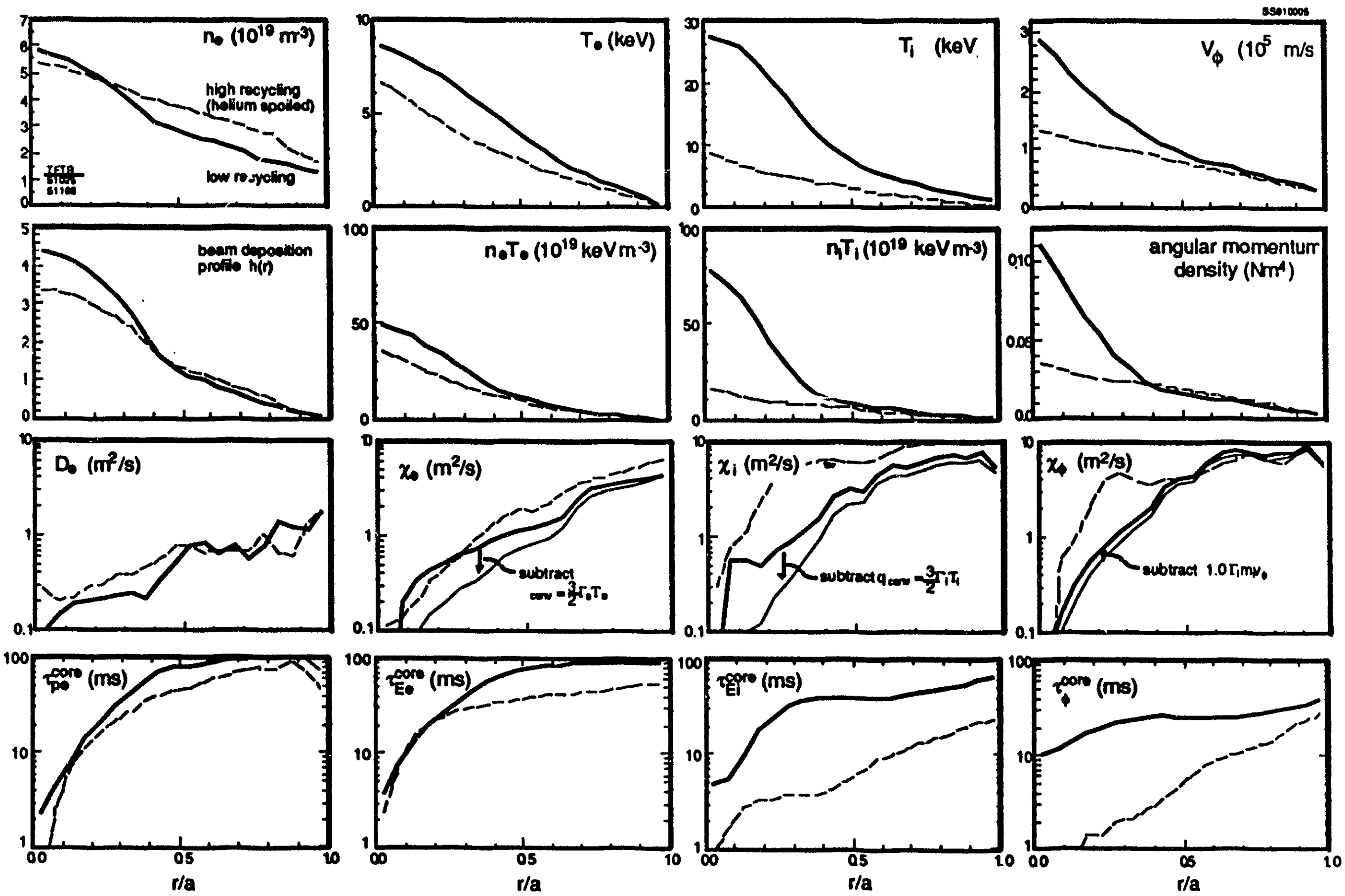

Figure 19: Comparison of particle, momentum and heat transport in TFTR 'supershot' versus L-mode plasmas with unbalanced injection (6 co-, 3 counter beams). Plasma conditions: R = 2.45 m, a = 0.8 m, B_T = 4.8 Tesla, I_p = 1.3 MA, The decrease in χ_ϕ is similar to that inferred for χ_i. Note that inferred χ_i decreases significantly if a convection term $q_{\rm conv} \equiv \frac{3}{2}\Gamma_i T_i$ is subtracted from the total ion radial heat flow. The corresponding changes in electron transport (D_e, χ_e, $\tau_{\rm pe}^{\rm core}$, $\tau_{\rm Ee}^{\rm core}$ are less than the changes in ion transport (larger improvemenent in electron confinements are observed in better-quality supershots with balanced injection [27]).

END

DATE
FILMED
12/23/91

I